PCCP

Accepted Manuscript

This is an *Accepted Manuscript*, which has been through the Royal Society of Chemistry peer review process and has been accepted for publication.

Accepted Manuscripts are published online shortly after acceptance, before technical editing, formatting and proof reading. Using this free service, authors can make their results available to the community, in citable form, before we publish the edited article. We will replace this *Accepted Manuscript* with the edited and formatted *Advance Article* as soon as it is available.

You can find more information about *Accepted Manuscripts* in the **Information for Authors**.

Please note that technical editing may introduce minor changes to the text and/or graphics, which may alter content. The journal's standard **Terms & Conditions** and the **Ethical guidelines** still apply. In no event shall the Royal Society of Chemistry be held responsible for any errors or omissions in this *Accepted Manuscript* or any consequences arising from the use of any information it contains.

Formation of Interconnected Morphologies via Nanorod Inclusion in Confined Assembly of Symmetric Block Copolymers

Jay Hoon Park[a] and Yong Lak Joo[a,]*

[a]School of Chemical and Biomolecular Engineering, Cornell University, Ithaca, NY, 14853

We have investigated the effect of nanorods on the symmetry breaking of a model diblock copolymer under cylindrical confinement using coarse-grained molecular dynamics. Unlike nanoparticles, nanorods can readily be interconnected with each other and also induce connection across self-assembly domains at much lower loading than nanoparticles. Such interconnecting nanorods, when incorporated within the nanofiber confined assembled block copolymer, have great potential to provide highly conductive pathways for energy applications, such as battery electrodes and separators. Symmetric block copolymers (BCP) under cylindrical confinement with nanorod aspect ratio (N)s of 1, 5, and 10 are examined with three different types of nanorod-BCP attraction: a) neutral nanorod, b) *A* (wall-attractive phase)-attractive nanorods, and c) *B* (wall-repulsive phase)-attractive nanorods. The system was studied with both selective and neutral wall, which affects the orientation of interconnected nanorod network. Upon close examination of the BCP/nanorod self-assembly, we have discovered that the ratio of interphase distance to nanorod aspect ratio (I/N) can be correlated to the onset of nanorod interconnectivity and formation of asymmetrical interconnected BCP morphology. By developing a phase diagram with respect to I/N, one can predict the formation of desired BCP morphology and the critical loading of nanorods for connected morphologies in cylindrical confinement.

Keywords: nanorod, block copolymer, cylindrical confinement, coarse-grained molecular dynamics

Introduction

Recent advances in nanoscale science have seen an ever increasing number of studies on nanoparticle/polymer composites aimed to significantly enhance the material properties. These material properties include optical,[1,2] mechanical,[3] electrical,[4,5] and thermal[6] properties which are inherited from the nanoparticles. In particular, nanoparticle/block copolymer (BCP) nanocomposites are known to assemble nanoparticles in a well-ordered or well-dispersed manner,[7] which is not easily achieved otherwise due to the tendency of nanoparticles to form aggregates. Such placement of nanoparticles is made possible by utilizing self-assembled BCP morphologies that are typically nanometers in size. Under cylindrical confinement, these BCPs can form unique morphologies that are not seen in bulk, such as concentric ring[8] and helix.[9,10] Most notably, Fredrickson and coworkers have investigated how these novel BCP morphologies can form under cylindrical confinement to yield composite mesostructures experimentally and theoretically.[11] This confined assembly of BCP is a well-known phenomenon as observed by many recent studies,[12-16] which is known to be a combined result of commensurability, polymer-surface condition, and the confining geometry. When nanoparticles are placed within such novel BCP structures under cylindrical confinement, an interconnected metal nanoparticle network can be formed. Sides *et al.* demonstrated that increasing the NP volume fraction in a symmetrical diblock copolymer can swell and distort the BCP domain, eventually leading to formation of asymmetrical morphologies such as inverse hexagonal cylinder to minimize interfacial energy.[17] Such BCP/nanoparticle nanocomposite structures under cylindrical confinement have been observed from both experiments [18] and simulation.[19] Kalra *et al.* electrospun symmetrical PS-*b*-PI mixed with Fe_2O_3 nanoparticle and successfully formed a bicontinuous BCP/nanoparticle

morphology under cylindrical confinement.[18] The BCP/nanoparticle morphologies were also verified in our recent coarse-grained molecular dynamics (CGMD) study.[19] Using simulations, we have predicted a series of BCP/nanoparticle morphologies varying parameters such as the confinement dimension, the nanoparticle-BCP interaction, wall selectivity, and nanoparticle loading.

Based on the good agreement between our simulation and experiment, we have attempted to expand our CGMD study to cylindrically confined BCP with anisotropical nanorods. Nanorods possess the same intrinsic material properties that nanoparticles have but often offer a greater enhancement in material properties when compared with same volumetric loading of nanoparticles.[20,21] Due to its anisotropy, the orientation entropy of nanorod becomes important in deciding its self-assembly within the polymer. There has been a few recent experimental and computational studies on self-assembly of nanorod/BCP in bulk. Most notably, He *et al*. inspected mobile nanorods in symmetrical and asymmetrical diblock copolymer films using the self-consistent field (SCF) theory and dissipative particle dynamics (DPD).[22] They found that the presence of nanorods can induce the formation of different morphologies near the surface and in the interior of the film. Experimentally, Thorkelsson *et al*. observed formation of aligned and continuous nanorod networks within BCP.[23] Through the connected network provided by nanorods, one can produce a nanomaterial with conductive pathways and superior material properties. Naturally, this well-ordered nanorod network may prove useful in photovoltaic devices, magnetic storage, and sensor applications. It is also possible to form connected nanorods with more directional freedom by leveraging bicontinuous BCP/nanorod self-assembly. The formation of such a network of nanorods in electrospun nanofibers can be even more

advantageous than in bulk or in film mainly due to the advantages of electrospinning process including superior productivity, ultrahigh surface area to mass ratio, substrate-free, and more variation of unique self-assemblies under cylindrical confinement. From our previous experiments[18] and simulations,[19] a bicontinuous BCP/nanoparticle morphology was observed under cylindrical confinement, thus we expect to see the formation of bicontinuous BCP/nanorod morphology as well. To our knowledge, no comprehensive study has been conducted on BCP/nanorod self-assembly under cylindrical confinement. From the complex interaction between nanorods, BCP, and the cylindrical walls, one could expect to observe drastically different self-assembly dynamics. Therefore, it is crucial to have a predictive tool that can provide a specific guideline on confined assembly of BCP/nanorods to efficiently create a desired nanostructure such as interconnected morphologies for the appropriate application.

To this end, we have employed CGMD to predict the self-assembly of nanorod/BCP under cylindrical confinement. Here, symmetrical BCP were confined to cylindrical channels with diameters (D) which are typically $1.0 - 4.0$ times greater than the BCP domain spacing, L_0. No significant effects of initial configurations on the final morphology were observed in the current study with moderate confinement conditions. In the past, Kalra *et al.* observed a distorted BCP morphology in electrospun fiber due to the combined effect of extensional flow and confinement.[18] After annealing, the BCP inside the electrospun fiber exhibited an equilibrium morphology as a result of BCP self-assembly under cylindrical confinement with selective interaction towards the silica wall surround the fiber.[18] Thus, it is important to examine the combined effects of flow and confinement on BCP/nanoinclusion self-assembly to accurately predict and understand the mechanism within the electrospun nanofibers. Since CGMD is often

used to predict polymer flow dynamics, it is the best method to investigate the combined effects. Our previous simulation had shown a good agreement between the electrospun experiment and the predicted simulation,[19] and we expect to predict the BCP/nanorod nanostructure under cylindrical nanopore confinement here. We have primarily investigated the BCP/nanoparticle morphologies from varying i) the confinement dimension (D/L_o), ii) nanorod selectivity, iii) wall selectivity, iv) nanorod aspect ratio (N), and v) nanorod volumetric loading. From the morphologies, we note the connectivity of the nanorods within polymer as well as the associated BCP morphology. From these results, we have constructed a phase diagram to elucidate the formation of bicontinous BCP/nanorod morphology under a given set of parameters, and how this result differs from bulk BCP and BCP/nanorod self-assembly.

Results and Discussion

Before inspecting the effect of cylindrical confinement, we first examine the effect of nanoparticle and nanorod inclusion in symmetrical BCP in bulk. We have denoted the A phase as blue, the B phase as green, and nanoparticles or nanorods as red. As shown in Figure 1a), symmetrical BCP forms the expected lamellae in bulk. Then 10 vol% nanoparticle and nanorods with N= 1, 5, 10 with a) A-domain selectivity (Figure 1b) and b) neutral selectivity (Figure 1c) were added to the bulk symmetrical BCP. In the case of the selective nanoparticles, we observe that nanoparticles are found in the selective blue domain, A. We note that the presence of selective nanorods (N = 5 and N = 10) enables formation of interconnected nanorod/A phase composite structure, which was not observed with spherical nanoparticles where the A lamellae phase was preserved. The rigid, anisotropic nanorods tend to form anisotropic order, especially with the longer nanorod with N = 10. This may possibly result in the nanorod forming a nematic

5

phase, which interferes with the BCP self-assembly and results in interconnected nanorod/*A*-phase composite structure. With neutral nanoinclusions, we observe that the nanoparticles and nanorods are primarily found along the interface between *A* and *B* phases. As these nanoinclusions do not affect the bulk *A* and *B* phases, the lamellae morphology is preserved for all nanoinclusions, in contrast to the selective nanoinclusions. Despite the preservation of the lamellae morphology, the neutral nanorods exhibit connectivity, potentially serving as a conductive bridge between the alternating interfaces.

We also studied the effect of cylindrical confinement on the BCP/nanorod self-assembly. First, the wall was set neutral towards both BCP phases and nanorods. Figure 2 shows the snapshot of 10 vol% nanoparticle/nanorod in symmetrical BCP under neutral cylindrical wall. It should be noted that the cylindrical wall phase has been removed in our figures for clarity. The nanoinclusions used here are either selective towards the *A* phase or neutral with $N = 1$ (nanoparticles), 5, and 10 (nanorods). The nanoparticles are primarily placed according to their chemical affinity as observed by the selective nanoparticles within the *A* phase and the non-selective nanoparticles at the interface between *A* and *B* phases. With a volumetric loading of 10%, we do not expect any change in BCP morphology from swelling of the nanoparticle-rich domain as observed in Figure 2. However, when N is increased to 5, BCP morphology evolves from symmetrically stacked disk morphology to axially connected BCP/nanorod morphology. As N is further increased to 10, more apparent interconnectivity and asymmetrical BCP morphology is induced. Unlike nanoparticles, each nanorod is connected with each other within the preferred domain due to its anisotropic orientation and rigidity, effectively providing a conductive path within the preferred domain. To induce completely connected nanorods within the cylindrically

confined BCP, the nanorods must be connected axially. This would require the selective nanorod to either be placed across the repulsive B domain or induce axially connected morphology of A domains. Our simulation results suggest that the latter is the case here with $N \geq 5$ inducing an asymmetrical BCP morphology. In the case of neutral nanorod, the axially connected nanorod does not necessarily require the formation of axially connected A or B morphology because the nanorod is not particularly repulsive to either phase. When $N \geq 5$, the nanorod aspect ratio is comparable to the periodic axial length of one A domain (~ 4.5). At this point, a single nanorod can act as a bridge between two interfaces which results in an interconnected nanorod network through the domains. We believe that this axial interconnectivity of nanorods does not solely rest on N, but also depends on the rigidity of the nanorod. The combined effects of the aspect ratio and the rigidity result in an anisotropic nematic nanorod structure. As with the bulk case, this nematic nanorod phase can affect the BCP self-assembly. This effect is more pronounced for the longer nanorod with $N = 10$, which shows a symmetry breakage between the BCP and result in formation of asymmetrical BCP morphologies as seen in Figure 2. It should also be noted that even neutral nanorods ($N = 5$ or 10) alter BCP morphology, which was not seen with bulk in Figure 1. Again, we hypothesize that the rigidity of nanorod and its aspect ratio relative to the interphase distance between A and B phases are responsible for the breakage of BCP symmetry.

Secondly, we incorporated a selective cylindrical wall around BCP/nanorod (Figure 3). The blue A phase is attracted to the wall, while the green B phase is repulsive against the wall. We examined three different types of nanoparticle/nanorod selectivity: i) nanorod-A attractive with nanorod-wall attractive, ii) neutral nanorod, and iii) nanorod-B attractive with nanorod-wall repulsive. The confinement dimension was also varied, with D/L_0 ratios of 1.0, 2.5, and 4.0,

respectively. As before, nanofillers with three different aspect ratios $N = 1$, 5, and 10 were employed. The nanoparticles ($N = 1$) are observed in their preferred domain without altering BCP morphologies, similar to the neutral wall case. With small D/L_0 of 1.0, the nanorods ($N = 5$ or 10) are found wrapping their respective selective domain in a spiral-like assembly. This diagonally connected arrangement of nanorods almost resembles a helix, which can form under cylindrical confinement when confinement dimension is commensurate with the BCP domain size. As D/L_0 becomes larger, we expect to see more layers of A and B domains, and hence more complex morphologies. This indeed is the case when D/L_0 is increased from 1.0 to 2.5, where we can see nanorods are axially connected within their selective domains. Since the confinement dimension is larger, the nanorods are not forced to form a helical-like network as seen in $D/L_0 =$ 1.0. When D/L_0 is increased from 2.5 to 4.0, however, we do not see a huge difference in the nanorod interconnectivity at a given N value regardless of their selectivity. We must keep in mind that the nanorods/nanoparticles are selectively placed with respect to their selectivity, and with the formation of alternating layers of BCP under cylindrical confinement, it is the radial interphase distance that the nanorods have to overcome to assemble in a bicontinuous fashion. When D/L_0 increased from 2.5 to 4.0, the number of alternating layers increased, but the interphase distance is not varied much.

In order to quantify the interphase distance, I, we have examined BCP morphological characteristics with three different nanoparticle/nanorod selectivity for $D/L_0 = 2.0$, 2.5, and 3.0 (Figure 4). We defined I to be the minimum distance required for the nanorods to connect one nanorod-attractive phase to another. Under most circumstances, the interphase distance will then be the radial distance from the center of one nanorod-selective domain to the center of another

closest nanorod-selective domain. For the *A*-attractive case shown in Figure 4a), *I* will then be the distance from the wall *A* phase and core *A* phase. Thus, *I* increases slightly when D/L_0 is increased from 2.0 to 3.0. When $D/L_0 > 3.0$, there are three layers of *A* and *I* decreases accordingly. This trend of radial gap growth and decay was also observed in our previous simulation with asymmetrical BCP under cylindrical confinement as D/L_0 is increased from 2.0 to 3.0 and 3.0 to 4.0.[16] For the *B*-attractive case with $2.0 \leq D/L_0 \leq 3.0$, there is only a single nanorod-attractive *B* phase that is radially sandwiched between core and wall nanorod-repulsive *A* phases. Hence, a relatively long interphase distance *I* is required to bridge the *B* domain through the core nanorod-repulsive *A* phase. This means that a nanorod would have to be as long as the diameter of the entire *B* domain, as described in Figure 4b. The *B* domain interphase distance becomes shorter as two *B* layers are formed when $D/L_0 > 3.0$. In the case of the neutral nanorods, the radial interphase distance is shorter than the selective ones because the nanorod-attractive domain is at the interface between *A* and *B* phases. This would cause the nanorods to form an interconnected network more easily at relatively lower loading than the selective ones.

Using the relationship between the interphase distance *I* and nanorod aspect ratio *N*, we have quantified the critical loading of nanoinclusions above which alternating layers are interconnected radially and axially, as shown on the right column of Figure 5. When $N = 1$, about 30 vol % is needed to break the symmetry of BCP and induce radially interconnected layers. When $N = 5$, the onset of radial interconnectivity is observed at a much lower loading of 15 vol %, which is a half of the nanoparticle loading required for the onset of radial connectivity. As *N* is further increased to 10, the interconnectivity is observed at even lower loading of 7.5 vol %. The phase diagram in the left column of Figure 5 depicts critical loading at which point one can

expect to see interconnected layers. The ratio of interphase distance to nanorod aspect ratio, I/N can be correlated to the onset of nanorod interconnectivity and formation of asymmetrical interconnected BCP morphology. There are two slopes that can describe the data sets. The left slope in the region of small I/N values, depicted by blue straight trend line in Figure 5, represents nanorod-like behavior, while the red line on the right in the region of small I/N values represents nanoparticle like behavior. According to this phase diagram, the nanorod loading required to interconnect nanorods are about 7.5%, compared to ~ 30% to 40 % for nanoparticles. This difference emphasizes the significance of the advantage of high aspect ratio nanorods to induce an interconnected nanorod network when compared with nanoparticles. It should be noted that the onset of interconnectivity is observed at higher concentration for bulk system, as depicted by the dotted lines. This difference is even greater for the nanorod-region, which was expected as the number of ways for the nanorods to interconnect is limited under confinement, and hence more likely to be interconnected at much lower loading than in bulk. It is also notable that the transition from nanorod-zone to nanoparticle-zone occurs when $I/N \sim 2$ for bulk, which is lower than the confined case ($I/N \sim 4$). This difference shows that nanorod-like behavior is observed with shorter nanorods under confinement than bulk, which can be advantageous in forming interconnected nanorod/BCP network.

The B-attractive nanorods show the similar trend as A- attractive case, where the onsets of radial interconnectivity are observed at 30 %, 15 %, and 7.5 % for $N = 1$, 5, and 10, respectively. We also note that although the phase diagram is very similar to the A- attractive case, the slope in nanorod-region is about 1.5 times steeper than the A-attractive counterpart. From this observation, if N is slightly decreased, the loading required increases more than the A-

attractive case. This is mainly because of the regions where there is one single *B* layer sandwiched by two *A* layers, as seen from Figure 4. Finally, for the neutral case, we know from Figure 4 that *I* is typically shorter than the selective nanorods at the same D/L_0. As such, the onset of interconnectivity when $D/L_0 = 4.0$ is at 5%, 10%, and 30 %, respectively for $N = 10$, 5 and 1, which is lower than the selective nanorods at $D/L_0 = 4.0$. The critical loading of neutral nanorods required for the interconnected network is much less than that of selective nanorods. For all of these cases, higher concentrations of nanorods were required to form interconnected nanorod/polymer morphologies in the bulk system.

Conclusions

In summary, we have predicted the self-assembly of BCP/nanorod nanocomposites under cylindrical confinement by considering the wall selectivity, nanorod-BCP selectivity, aspect ratio, and nanorod concentration. We have found that as the aspect ratio *N,* becomes comparable to the interphase distance *I*, the nanorods are interconnected axially if confined within a neutral wall, and radiallly if confined within a selective wall. Specifically, we have determined at which points we can expect to observe bicontiuous BCP/nanorod assemblies, or nanorods that are interconnected both radially and axially. We observed that the interconnected nanorod network can form at much lower concentrations under confinement than in bulk. We also observed that shorter nanorods can exhibit more nanorod-like behavior under confinement than in bulk. The constructed phase diagram based on the ratio of interphase distance and the nanorod aspect ratio should serve as a good guideline to determine the critical loading and aspect ratio of nanorods for

desired confined assembly. By controlling the interconnected morphologies at will, we may be able to efficiently tune important properties of the composites such as ionic and electrical conductivities and mechanical strength for sensory, photovoltaic, and magnetic storage applications.

Simulation Methods

Block copolymer Modeling: The model block copolymer chains in the current coarse-grained MD study consist of minor (A) and major (B) blocks of monomers. Within a polymer chain, the neighboring monomers are connected by a finitely extensible nonlinear elastic (FENE) potential,

$$u^{FENE}(r) = -\frac{1}{2}kR_{max}^2 \ln\left[1-\left(\frac{r}{R_{max}}\right)\right],$$ (1)

where the spring constant k is 30, and the maximum extensibility R_{max} is 1.5, as used by Kremer and Grest to simulate polymer beads.[24] Monomers in each block are modeled by Weeks-Chandler-Anderson (WCA) potential[25],

$$u^{REP}(r) = 4\varepsilon\left[\left(\frac{\sigma}{r}\right)^{12} - \left(\frac{\sigma}{r}\right)^6\right] + \varepsilon = u^{LJ}(r) + \varepsilon, r \leq 2^{1/6}$$

$$u^{REP}(r) = 0, r > 2^{1/6}$$ (2)

where r is the separation distance between beads, and and are the Lennard Jones parameters. It should be noted that the monomer models have excluded volume interactions between them. An attractive potential between like monomers (i.e., *A-A* or *B-B*) was used to incorporate the physics of microphase separation between the *A* and *B* species. The attractive potential, as described by

Horsch et al.[26] to model the equilibrium properties of diblock copolymer melts, is again a LJ potential but now it is cut and shifted at values that differ from those presented in Equation (2).

$$u^{ATT}(r) = 4\varepsilon\left[\left(\frac{\sigma}{r}\right)^{12} - \left(\frac{\sigma}{r}\right)^{6}\right] + u^{LJ}(2.5), r \leq 2.5,$$
$$u^{ATT}(r) = 0, r > 2.5$$

(3)

The higher cutoff means that this is not purely repulsive and that monomers of the same type are attracted to each other. The thermostat used was dissipative particle dynamics (DPD) thermostat. We point the readers to the previous simulation work done by Kalra *et al*. to learn more about the potentials and thermostat used.[27] The chain length of polymer, *M*, was fixed at ten beads throughout the simulations. Each phase was assigned with five beads, i.e. *A:B* = 5:5. The site density ρ and the temperature k_BT were kept fixed at 0.85 and 1.0, respectively. The number of beads in a fixed box size was determined based on the site density.

Nanoparticle Modeling: The nanoparticle size was set at 1 in MD units, which is equivalent to nanoparticles size of ~ 1 nm in this system where BCP is described by a bead-spring polymer chain with 10 beads. The size of nanoparticle ensured that the results were not peculiar to the particle size of one Kuhn monomer.[27] When the simulation results were compared with the experimental results, the nanoparticle fractions were chosen to match the experimental setup. The nanoparticle attraction towards *A*, *B*, and wall phases were all varied to match *A*-attractive, *B*-attractive, and neutral nanoparticle. A fixed number, *N*, of spherical nanoparticle beads were bound together to form a nanorod with aspect ratio of 1~10. In addition to the FENE model used to bind the beads together, a three-body angular potential was adopted [28] to model the rigidity of the nanorod:

$$U_{ijk} = \frac{1}{2}k_\theta(\theta_{ijk} - \theta_{eq})^2 \tag{4}$$

where θ_{ijk} is the angle between three adjacent beads, θ_{eq} is the desired equilibrium angle, and k_θ is the constant which can be used to modify the rigidity of the rod. To form "stiff" nanorod, k_θ was typically set at 7.

Wall Modeling: To apply the cylindrical confinement on the diblock copolymer, a fixed cylindrical wall diameter was set in x and y directions. Immobile beads with diameter of 1 MD unit were aligned cylindrically on the BCP and BCP-nanoparticle to set up the wall. Thus, periodic boundary condition was only applied in the axial z direction. The diameter of wall was set to be ranging from 9.1 to 36.4, which is about 1 to 4 times bigger than the polymer domain spacing (~9.1). The cylindrical wall layer was given attraction potential to the *A* phase. If the nanoparticle prefers the *A* phase over the *B* phase, they are set to be attracted towards wall as well. When the nanoparticle prefers the *B* phase, however, the nanoparticle is repulsive from the wall. The strength of attraction of nanoparticle towards wall and phase *A* is set to be the same.

Simulation Details: The velocity Verlet algorithm was used to integrate the equations of motion. The MD integration time step size, Δt, was fixed at 0.01. A cell list algorithm was used to make the code efficient,[29] and the cutoff was set to be 2.5. To prevent undue periodic boundary artifacts, we varied the radius and height (z-axis length) of the system until stacked disk morphology was attained. When the dimensionless periodic height of the box size, L_Z, was set at 9.54, the system attains the most stable form of stacked disk at equilibrium. For the dimensions of radii we used in this study, the aforementioned L_Z values attained the equilibrium structure.

Table I. Variables used in MD simulation

Parameters	Symbol	Value(MD units)
Temperature	k_BT	1
Monomer size	σ	1
nanoparticle diameter	σ_p	1
nanoparticle monomer mass	m	1
Nanorod aspect ratio	N	1,5,10
Bead density	ρ	0.85
Diameter of cylindrical confinement	D	9.1~36.4
Z-axis periodic length	L_z	9.54
Flory-Huggins parameter*N	χN	53.3
MD integration time step	Δt	0.005
Length of polymer domain	L_0	~ 9.1

The simulations were run for a sufficiently long time until variables such as pressure, potential energy, radius of gyration, and mean squared end-to-end distance remained constant. The order parameter, O, which is the largest eigenvalue of the Saupe tensor,[30] was monitored and stabilized along with the other variables when MD time was approximately 2000, which is about 4,000,000 time steps for our simulation. The parameters used in this system are summarized in Table I.
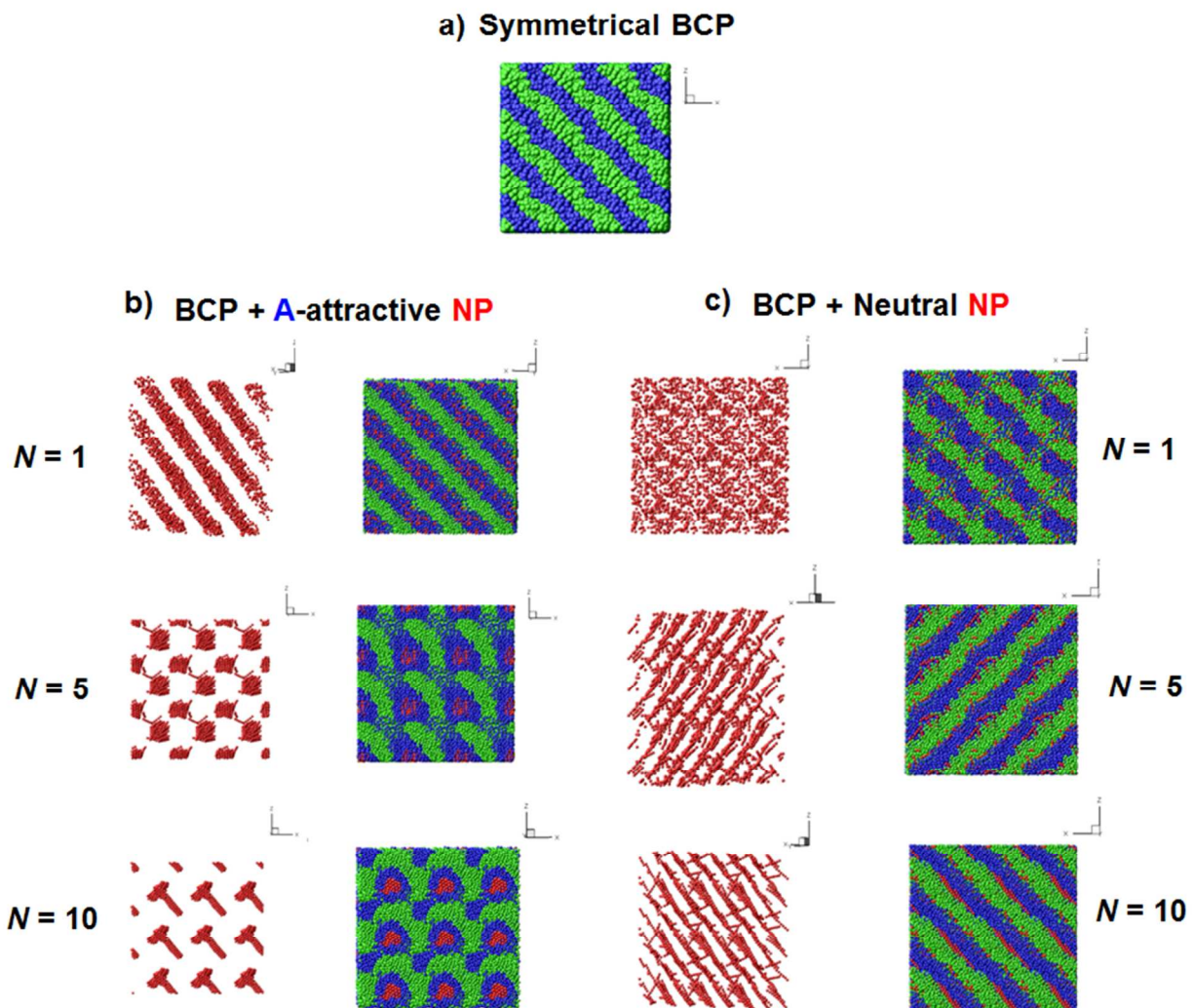
Acknowledgements

Figure 1. Snapshot of a) pure symmetrical BCP, b) BCP and A-attractive 10 vol% nanoparticles and nanorods, and c) BCP and neutral nanoparticles and nanorods in bulk system. The nanoparticle and nanorods are shown with BCP phases blanked out on left columns for b) and c).
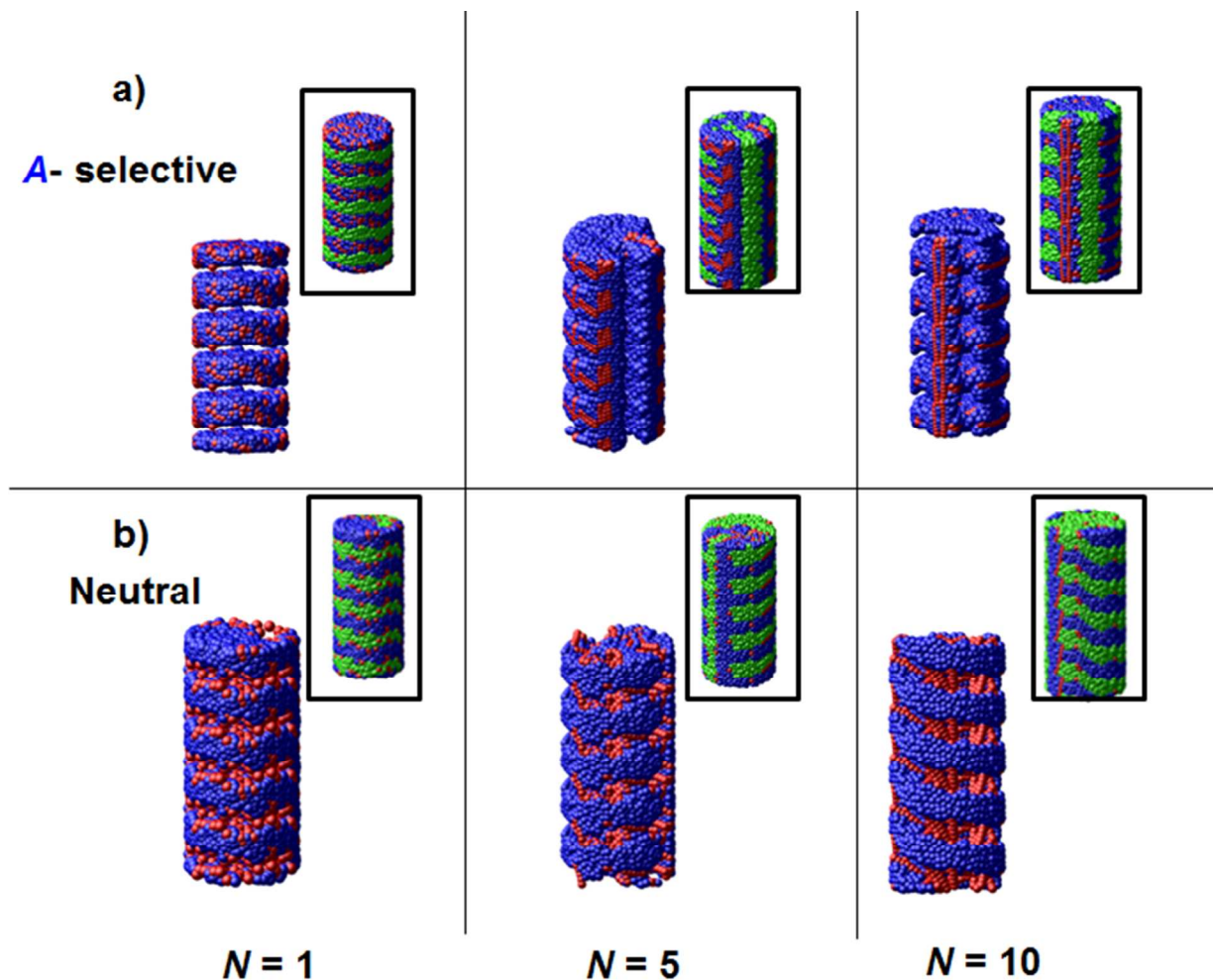
Figure 2. Snapshot of 10 vol% of nanorod with BCP under with neutral cylindrical wall (not shown). The top rows a) show selective nanorod (attracted to blue *A* phase) while the bottom row b) shows neutral nanorods. The aspect ratio is increased from 1, 5, and 10 from left to right. The 3-D morphology is shown with green *B* phase blanked out. The inset shows the full 3-D morphologies. D/L_0 is fixed at 2.5.
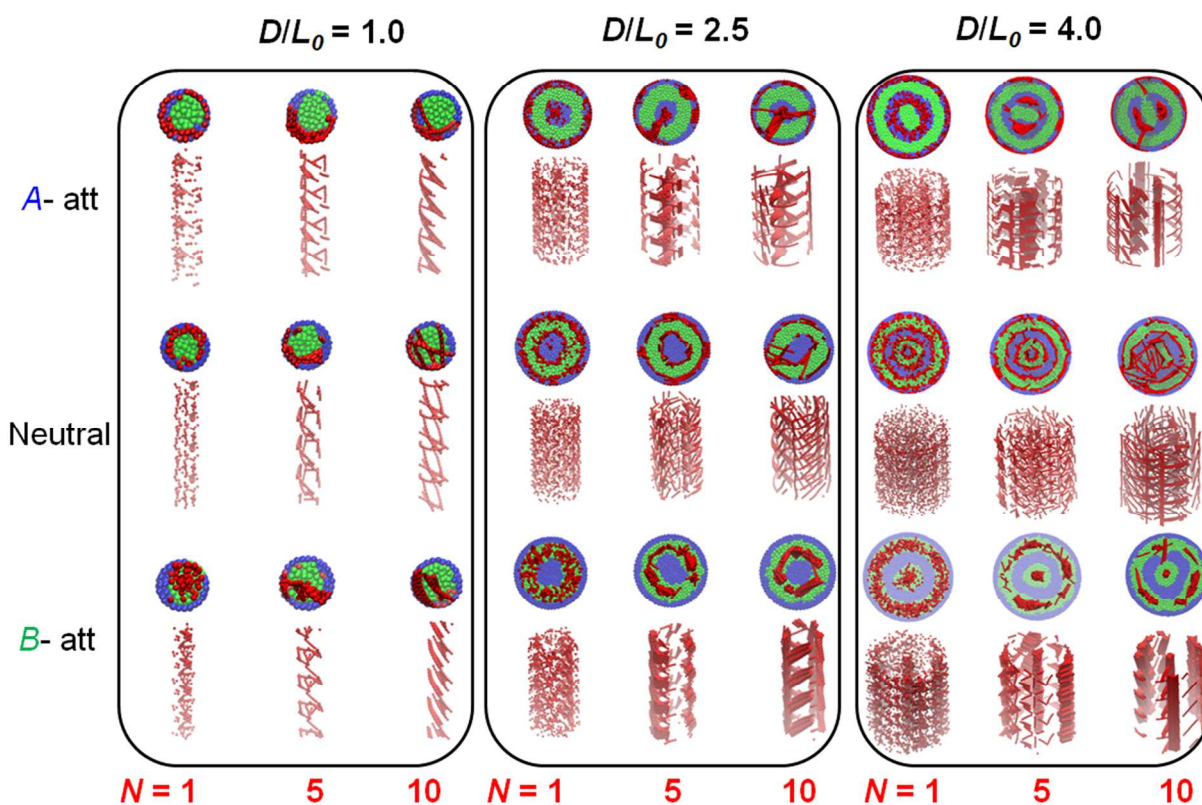
Figure 3. Snapshot of 10 vol% of nanorod with BCP under with *A*-selective cylindrical wall (not shown). The top rows a) show *A*- selective nanorod (attracted to blue *A* phase) the middle row b) shows neutral nanorods, and the bottom row c) shows B-attractive nanorods. The aspect ratio is increased from 1, 5, and 10 from left to right. The 3-D morphology is shown with green *B* phase blanked out.
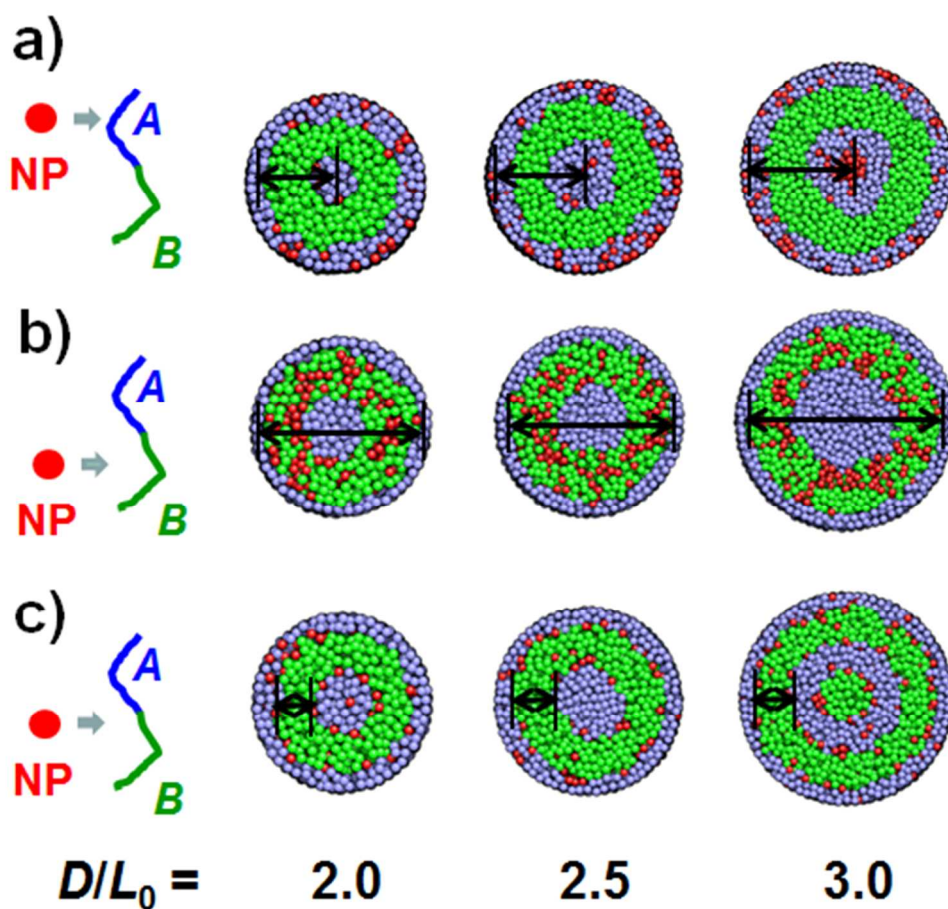
Figure 4. Definition of the interphase distance as indicated by black line for *A*-attractive nanorod, *B*-attractive nanorod, and neutral nanorods with D/L_0 = 2.0, 2.5, and 3.0.
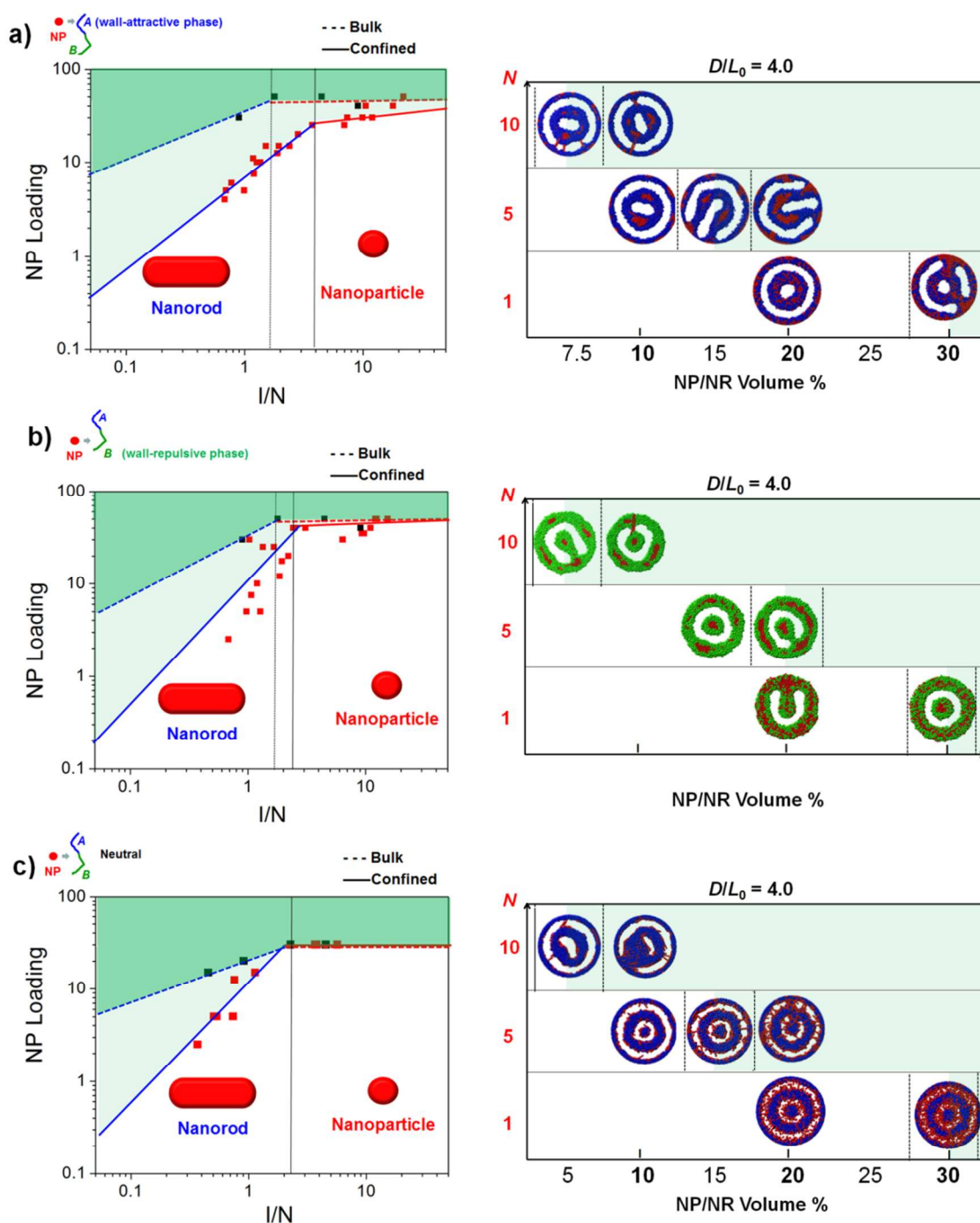
Figure 5. Phase diagram of a) *A*-attractive, b) neutral, and c) *B*-attractive, nanoparticle/nanorods with symmetrical BCP. The x-axis represents *I*/*N*, interphase distance over aspect ratio, while the y-axis represent the nanoparticle loading. The black squares (dotted line) represent the bulk data, while the red squares (solid line) represent the confined assembly data. On the right, the BCP/nanoparticle or BCP/nanorod morphologies are shown with respect to nanoparticle/nanorod volume % and *N* at *D*/*L₀* = 4.0.

References

1   C. Sönnichsen, T. Franzl, T. Wilk, G. von Plessen, J. Feldmann, O. Wilson, and P. Mulvaney, *Phys. Rev. Lett.,* 2002, **88**, 077402..

2   J. Pérez-Justea, I. Pastoriza-Santosa, L. M. Liz-Marzána, and P. Mulvaney, *Coordination Chemistry Reviews,* 2005, **249**, 1870-1901.

3   J. N. Coleman, U. Khan, and Y. K. Gun'ko, *Adv. Mater.* 2006, **18**, 689-706.

4   C. Min, X. Shen, Z. Shi, L. Chen, and Z. Xu, *Polymer-Plastics Technology and Engineering*, 2010, **49**, 1172–1181.

5   W. U. Huynh, J. J. Dittmer, and A. P. Alivisatos, *Science,* 2002, **295**, 29.

6   A. M. Marconnet, N. Yamamoto, M. A. Panzer, B. L. Wardle, and K. E. Goodson, *ACS Nano,* 2011, **5**, 4818–4825.

7   A. C. Balazs, T. Emrick, and T. P. Russell, *Science*, 2006, **314**, 1107.

8   K. Shin, H. Xiang, S. I. Moon, T. Kim, T. J. McCarthy, and T. P. Russell, *Science,* 2004, **306**, 76.

9   M. Kamperman, L. T. J. Korley, B. Yau, K. M. Johansen, Y. L. Joo, and U. Wiesner, *Polymer Chemistry,* 2010, **1**, 1001-1004.

10   M. L. Ma, E. L. Thomas, and G. C. Rutledge, *Macromolecules* 2010, **43**, 3061-3071.

11   Q. Wang, in Nanostructured Soft Matter: Experiment, Theory, Simulation and perspectives, Ed. A. V. Zvellindovsky, Springer, Bristol, UK, 2007.

12   Y. Wu, G. Cheng, K. Katsov, S. W. Sides, J. Wang, J. Tang, G. H. Fredrickson, M. Moskovits, and G. D. Stucky, *Nat. Mater.* 2004, **3**, 816-822.

13   T. Iwama, N. Laachi, K. T. Delaney, B. K. Kim, S. M. Hur, R. Bristol, D. Shykind, C. J.

Weinheimer, and G. H. Fredrickson. *J. Photopoly,.Sci. Technol.* 2013, **26**, 15-20.

14 C. R. Stewart-Sloan and E. L. Thomas*, Eur. Polym. J.* 2011, **47**, 630-646.

15 A-C. Shi and B. Li, *Soft Matter*, 2013, **9**, 1398-1413.

16 A-C. Shi and B. Li, in *Polymer Science: A comprehensive reference*, ed. K. Matyjaszewski and B. Moller, 2012, **7**, 71-81.

17 S.W. Sides, B.J. Kim, E.J. Kramer and G.H. Frederickson, *Phys. Rev. Lett.* 2006, **96**, 250601.

18 V. Kalra, J. Lee, J. H. Lee, S. G. Lee, M. Marquez, U. Wiesner, and Y. L. Joo, *Small,* 2008, **4**, 2067.

19 J. H. Park, V. Kalra, and Y. L. Joo, *Soft Matter,* 2012, **8**, 1845-1857.

20 G. Peng, F. Qiu, V. V. Ginzburg, D. Jasnow, and A. C. Balazs, *Science,* 2000, **288**, 1802.

21 G. A. Buxton and A. C. Balazs, *J. Chem. Phys*., 2002, **117**, 7649.

22 L. He, L. Zhang, H. Chen, and H. Liang, *Polymer,* 2009, **50**, 3403.

23 K. Thorkelsson, A. J. Mastroianni, P. Ercius, and T. Xu, *Nano Lett.,* 2012, **12**, 498−504.

24 K. Kremer and G. S. Grest, *J. Chem. Phys*., 1990, **92**, 5057.

25 J. D. Weeks, D. Chandler, and H. C. Anderson, *J. Chem. Phys.*, 1971, **54**, 5237.

26 M. A. Horsch, Z. Zhang, C. R. Iacovella, and S. C. Glotzer, *J. Chem.Phys.,* 2004, **121**, 11455.

27 V. Kalra, S. Mendez, F. Escobedo, and Y. L. Joo, *J. Chem. Phys.,* 2008, **128**, 164909.

28 A. Maiti, J. Wescott, and P. Kung, *Mol. Simulat.*, 2005, **31**, 143.

29 M. P. Allen and D. J. Tildesley in *Computer Simulation of Liquids* Oxford University Press, New York, 1987.

30 P. G. DeGennes in *The Physics of Liquid Crystals*, 2nd Eds; Oxford University Press, New York, 1993.

31 M. Tarini, P. Cignoni, and C. Montani, *IEEE Transactions on Visualization and Computer Graphics.*, 2006, **12**, 1237-1244.